MedCrave
Step into the World of Research

Fluid Mechanics Research International Journal

Review Article

Open Access

CrossMark

Simulation based engineering science in fluid mechanics

Abstract

Industry practices have changed drastically in the recent decade or two by adapting computer aided methods leaving the approximate methods for design analysis practiced during the 20th century. The governing multi-physics fluid flow equations are stated and the need to find solutions using current platform approach is given. Two cases of complex problems concerned with Magnetohydrodynamic flow and aero-acoustics are addressed here using Simulation based engineering science (SBES) approach.

Keywords: SBES, fluid flow, magnetohydrodynamics, aero-acoustics

Volume 2 Issue 3 - 2018

JS Rao
President of the vibration institute of India, India

Correspondence: Prof. JS. Rao, president of the vibration institute of India, 1039, 2nd cross road, block II, Vidyaranyapura, Bangalore 560097, India, Tel +91 98453 46503, Email rao_js@yahoo.com

Received: May 07, 2018 | **Published:** May 29, 2018

Abbreviations: SBES, simulation based engineering science; MHD, magnetohydrodynamics; CFD, computational fluid dynamics; RANS, reynolds averaged navier stokes; NASA, national aeronautics and space administration; NSF, national science foundation; NIH, national institutes of health; NIST, national institute of standards and technology; HPC, high performance computing; CAD, computer aided design; LES; large eddy simulation; DES, detached eddy simulation

Introduction

Leonhard Euler (1707-1783), proposed Euler equations for the first time in 1757 which describe conservation of momentum for an inviscid fluid, and conservation of mass.[1] Claude Louis Marie Henry Navier[2] (1785-1836) and George Gabriel Stokes[3] (1819-1903) introduced viscous transport into the Euler equations, which resulted in the Navier-Stokes equation.[2,3] This forms the basis of modern day CFD (computational fluid dynamics). Faraday[4] discovered in 1831 that by moving a magnet next to a closed electric circuit, an electric current could be "induced" to flow in it. Electromagnetic induction is the principle behind electric generators, transformers and many other devices.

Reynolds[5] in 1894 is the first one to make a beginning of scientific experiments and discussed turbulence in the flow. Magnetohydrodynamics (MHD) involves study of magnetic fields and fluid flows and their interaction. Alfven[6] in 1942 was the first to introduce the term. Navier-stokes equations are combined with Alfven's MHD flow; they become important in large magnetic fields such as fusion reactors.[7] Because of Mesh size required in MHD flows, SBES becomes important in the solution of navier-stokes equations with electromagnetic effects.

Aero-acoustics is the primary cause of uncomfortable noise in cavity induced flows or helmholtz resonators in automotive and aerospace applications. When reynolds number is high, the flow becomes turbulent and unsteady and to get a numerical solution, the state quantities are decomposed into the mean and fluctuating parts that lead to reynolds equations. For the purpose of numerical computation, these equations are averaged, reynolds averaged navier-stokes (RANS) equations, with development of various turbulence models. The wave equation governs the transmission of acoustic pressure and wave propagation takes place in a sphere. Lighthill[8] in 1954 presented the acoustic analogy to account for the source terms. An extension of Lighthill's analogy is by Ffowcs Williams et al.[9] as given in 1969 that includes influence of arbitrary moving surfaces on sound generation. Eddies shed by turbulent flow typically generate Quadrupoles that form the sources for sound propagation.

The steam turbine and dynamo were invented in 1882 and the rotating machinery made an impact on the modern life styles and everyone wanted electric power. Road and air transportation became common and design became an essential part of design.

The design process essentially consists of two parts, the first one in making the baseline and then the second part on the application of science to make an analytical design. In the analytical design part professor Timoshenko made highly innovative contribution to the world of education by evolving approximate engineering approach in the early 20th century in the absence of number crunching ability from the digital computers.[10] The needs of exploding design were met using this approach together with testing and usage of factors such as stress concentration factor, factor of safety etc.

During the II world war, the first digital computer was born in Philadelphia that gradually changed the world of computation from Log Tables and Slide Rules. The digital computers gradually replaced the time consuming and testing intensive approximate engineering design approach, the mainstay of 20th century industrial practice by a direct Science to Engineering approach through simulation and high performance computing (HPC). Industry was quick to adapt this approach to cut the design time and costs.

United States of America was concerned with the need to introduce SBES. A high level panel was set up as a Presidential initiative with six government departments, National science foundation (NSF), department of energy (DOE), national aeronautics and space administration (NASA), national institutes of health (NIH), national institute of standards and technology (NIST) and department of defense (DOD), (see WTEC – panel report (2009) http://www.wtec.org/sbes/SBES-GlobalFinalReport.pdf). This report says on p.79, that "The use of simulation and computational models is pervasive in almost every engineering discipline and at every stage in the life cycle of an engineered system. Typical examples of the use of simulation in engineering include manufacturing process modeling; continuum

models of bulk transformation processes; structural analysis; finite element models of deformation and failure modes; computational fluid dynamics for turbulence modeling; multi-physics models for engineered products; system dynamics models for kinematics and vibration analysis; modeling and analysis of civil infrastructures; network models for communication and transportation systems; enterprise and supply chain models; and simulation and gaming models for training, situation assessment, and education."

Essentially, there are only basic sciences; solid mechanics, fluid mechanics, thermodynamics, heat transfer and electromagnetism as given in 17th and 18th centuries; they are all expressed as coupled partial differential equations. These equations can all be simulated using numerical methods. This simulation has become possible with the advent of digital computers for different domains of engineering as illustrated in Figure 1.

Initially dedicated computer programs were developed in research institutions which paved their way to commercial computer codes by turn of 20th century. They were first single physics codes. In modern fluid mechanics practices today, the flow path is first CAD modeled followed by meshing before applying the boundary conditions and setting up the numerical problem to be solved by a solver. The architecture of single physics codes is illustrated in Figure 2. The post-processor displays a nearly complete exact picture of velocities, temperatures, pressures, densities etc.

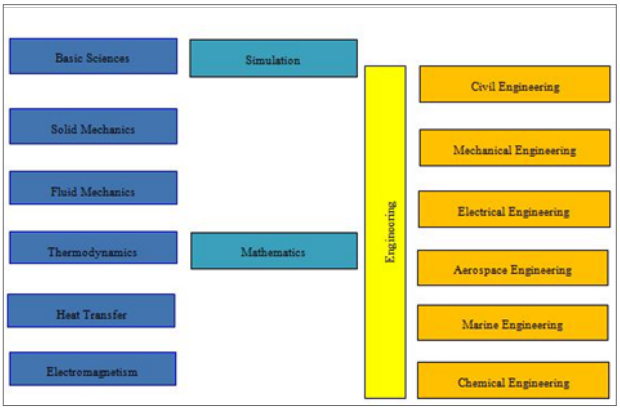

Figure 1 Science to engineering chart.

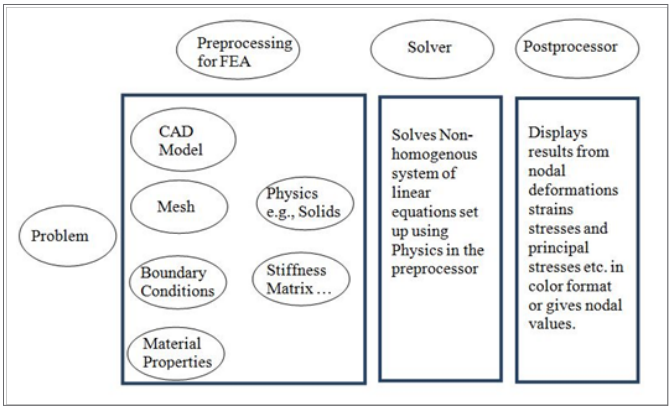

Figure 2 Single physics codes architecture chart.

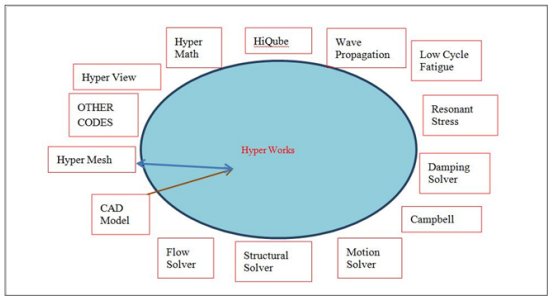

Figure 3 Chart for platform approach.

Industrial designs are not based on single physics and they are based on multiphysics. Therefore a Platform approach is adopted with multi-physics concepts, as outlined in Figure 3 by combining different single physics codes using codes such as TCL/TCK or Python.

SBES today helps in providing practical solutions of multi-physics flows. Some of these dealing with MHD flows and heat transfer and aero-acoustics are presented in this paper.

Governing equations for magnetohydrodynamic flow

The hydrodynamic governing equations are the mass (continuity), momentum and energy equations.[7] They are

$$\frac{\partial \rho}{\partial t} + \nabla \cdot \rho \mathbf{V} = 0 \tag{1}$$

$$\frac{\partial \mathbf{V}}{\partial t} + (\mathbf{V} \cdot \nabla)\mathbf{V} = -\frac{1}{\rho}\nabla p + \nu \nabla^2 \mathbf{V} + S \tag{2}$$

$$\rho C_p \left[\frac{\partial T}{\partial t} + (\mathbf{V} \cdot \nabla)T\right] = k\nabla^2 T + q''' \tag{3}$$

In equation (1) ρ is the density of the fluid and $\mathbf{V}$ is the velocity represented by $\mathbf{V} = ui + vj + wk$. The first term on the left is the accumulation/unsteady term which can be neglected for steady state condition and second term on the left is mass flux term. In equation (2) v is the kinematic viscosity, p is the pressure. The first term on the left is the unsteady term and the second term on the left is the convection term. The first term on the right is the pressure force term; the second term on the right is the diffusion term which is due to the viscous effects. The third term on the right is the source term which includes other forces such as gravitational forces, electromagnetic forces etc. In equation (3) k is the thermal conductivity, T is the temperature and C_p is the specific heat of the fluid. The first term on the left is the unsteady term and the second term on the left is the convection term. The first term on the right is the diffusion term. The next term is the volumetric heat generation q'''.

The equations given above are generic equations and what differentiates the equation when used for laminar and turbulent flow regimes is the replacement of molecular viscosity, v and thermal conductivity, k by effective viscosity, ν_{eff} and effective thermal conductivity, k_{eff} in the momentum and energy equation when the flow is turbulent.

$$\nu_{\text{eff}} = \nu_{\text{m}} + \nu_{\tau} \tag{4}$$

$$k_{\text{eff}} = k_{\text{m}} + k_{\tau} \tag{5}$$

Where ν_{τ} is the turbulent viscosity which is the increment in momentum transfer due to diffusion created by turbulence and k_{τ} is the turbulent thermal conductivity which is the increment in heat transfer due to diffusion created by turbulence.

The effect of magnetic field will be included by addition of Lorentz force term $j \times B$ and force due to electric charge $\rho_c E$ as a source term in the momentum equation and inclusion of joule dissipation term $\frac{j^2}{\sigma}$ as a volumetric heat generation term in the energy equation. The effect of magnetic field on turbulence can be included by altering the turbulent viscosity and turbulent thermal conductivity in the momentum and energy equation respectively. The modified momentum equation including the magnetic effects is given by

$$\frac{\partial \mathbf{V}}{\partial t} + (\mathbf{V} \cdot \nabla)\mathbf{V} = -\frac{1}{\rho}\nabla p + \nu \nabla^2 \mathbf{V} + \frac{1}{\rho}(j \times B) + \frac{1}{\rho}(\rho_c E) + S \qquad (6)$$

The modified energy equation including the Joule dissipation is given by,

$$\rho C_p \left(\frac{\partial T}{\partial t} + (\mathbf{V} \cdot \nabla)T \right) = k \nabla^2 T + \frac{j^2}{\sigma} + q''' \qquad (7)$$

The inclusion of new variables *j, E* and *B* in the hydrodynamic equations requires closure equations given using Maxwell's equations

$$\nabla \cdot D = \rho_c \qquad (8)$$

$$\frac{\partial B}{\partial t} = -\nabla \times E \qquad (9)$$

$$\nabla \cdot B = 0 \qquad (10)$$

$$\nabla \times H = j + \frac{\partial D}{\partial t} \qquad (11)$$

and Ohms law

$$j = \sigma(E + \mathbf{V} \times B) \qquad (12)$$

where *D* is the electric displacement. The above equations (1), (6)-(12) can be used for a range of problems, but the equations are complex and may not be fully modeled to capture the physics of liquid metal flows and heat transfer as in fusion reactors.

In applications where the flow velocity $|\mathbf{V}|$ is low as compared to the speed of light *c*, the force due to electric charge $\rho_c E$ can be neglected when $|\mathbf{V}| << c$ based on

$$\frac{|\rho_c E|}{|j \times B|} \approx \frac{|\mathbf{V}|^2}{c^2} \qquad (13)$$

This approximation will eliminate the inclusion of the term $\partial D/\partial t$ from equation (11) and equation (8) can be ignored when $u << c$. Using $B = \mu^* H$ and combining (11) and (12)

$$\frac{1}{\sigma \mu^*}(\nabla \times B) = (E + \mathbf{V} \times B) \qquad (14)$$

Considering $\nabla \times$ of equation (14) assuming is constant $\eta^* = \frac{1}{\sigma \mu^*}$, we have

$$\eta^* \left\{ \nabla(\nabla \cdot B) - \nabla^2 B \right\} = \nabla \times E + \nabla \times (\mathbf{V} \times B) \qquad (15)$$

Using (9) and (10), (15) becomes

$$\frac{\partial B}{\partial t} = \nabla \times (\mathbf{V} \times B) + \eta^* \nabla^2 B \qquad (16)$$

Equation (16) is the magnetic induction equation; the first term on the right is the induction term and the second term the diffusive term. The induction term describes the interaction of the field with flow. Magnetic Reynolds Number Re_m is the ratio of the momentum diffusivity to the electromagnetic diffusivity defined by

$$\mathrm{Re}_m = \frac{\text{Momentum Advection}}{\text{Magnetic Diffusion}} = \frac{\mathbf{V}_0 L}{\frac{1}{\mu^* \sigma}}$$

Where, μ^* is the fluid magnetic permeability (h/m). It characterizes the effect of induced magnetic field on the resultant magnetic field due to the imposed and induced magnetic fields. At $\mathrm{Re}_m << 1$ the imposed magnetic field will guide the flow and will be independent of the induced magnetic field as it will be very small compared to the imposed magnetic field. Equation (16) then becomes

$$\frac{\partial B}{\partial t} = \eta^* \nabla^2 B \qquad (17)$$

$$j = \frac{1}{\mu^*}(\nabla \times B) \qquad (18)$$

A summary of equations used for liquid metal flows involving heat transfer in presence of magnetic field is given below namely, mass, momentum, energy and magnetic induction.

$$\frac{\partial \rho}{\partial t} + \nabla \cdot \rho \mathbf{V} = 0 \qquad (19)$$

$$\frac{\partial \mathbf{V}}{\partial t} + (\mathbf{V} \cdot \nabla)V = -\frac{1}{\rho}\nabla p + \nu \nabla^2 \mathbf{V} + \frac{1}{\rho}\left[\frac{1}{\mu^*} B \cdot \nabla B - \nabla\left(\frac{B^2}{2\mu^*} \right) \right] + S \qquad (20)$$

$$\rho C_p \left(\frac{\partial T}{\partial t} + (\mathbf{V} \cdot \nabla)T \right) = k \nabla^2 T + \frac{\left(\frac{1}{\mu^*}(\nabla \times B) \right)}{\sigma} + q''' \qquad (21)$$

$$\frac{\partial B}{\partial t} = \eta^* \nabla^2 B \qquad (22)$$

The total number of unknowns is 9 including three scalars of velocity, three scalars of magnetic field, pressure, density and temperature and the number of equations is 8 including continuity, 3 momentum equations, energy and 3 induction equations. We need a closure equation for the set of equations. If the flow is incompressible then we can treat density as constant and hence removing the need of an extra equation. If the flow is compressible then we can use an equation for pressure as a function of temperature and density i.e., $p = f(T, \rho)$ for example like ideal gas law for gases.

MHD covers phenomena in electrically conducting fluids, where the velocity field V, and the magnetic field *B* are coupled. Any movement of a conducting material in a magnetic field generates electric currents *j*, which in turn induces a magnetic field. Each unit volume of liquid having *j* and *B* experiences MHD force $j \times B$, known as the Lorentz force *F,* see Figure 4. This force is to be included in Navier-Stokes equations.

In MHD flows in blanket channels of a Fusion reactor, interaction of the induced electric currents with the applied plasma-confinement magnetic field results in the flow opposing Lorentz force that may lead to high MHD pressure drop, turbulence modifications, changes in heat and mass transfer and other important MHD phenomena. In Fusion Reactors the magnetic field may be as much as 1.5 T. Hartmann[11] studied theoretically for the first time laminar flow of electrically conductive liquid, Mercury, in a homogeneous magnetic

field followed by an experimental study of the same by Hartmann et al.[12] A non-dimensional number is defined by Hartmann, denoted by Ha,

$$\mathrm{Ha} = \left(\frac{\text{Electromagnetic Forces}}{\text{Viscous Forces}}\right)^{\frac{1}{2}} = B_0 L\sqrt{\frac{\sigma}{\nu\rho}} \qquad (23)$$

Where, B_0 is the magnetic field intensity (Tesla), σ is the electrical conductivity of the fluid (1/Ωm) and ν is the kinematic viscosity of the fluid (m^2/s^2). For liquid metal flows in fusion reactors, the typical values encountered for Ha are of the order 2×10^4 and the effect of viscosity and turbulence on the flow is negligible in those situations.

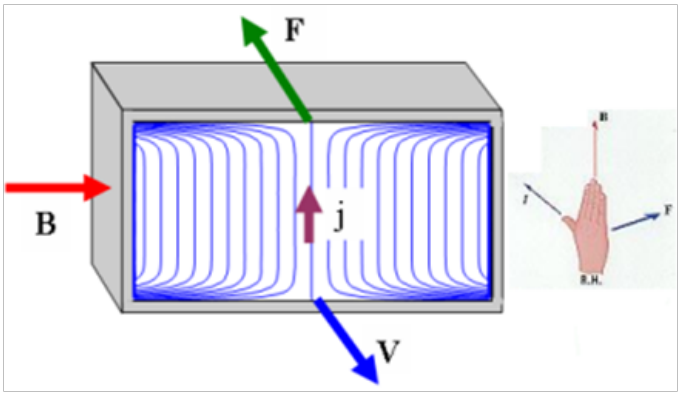

Figure 4 Relationship between magnetic field, electric current, velocity field and lorentz force.

Hartmann analytical solution for a MHD flow in a duct is shown in Figure 5. If Ha grows, the velocity profile becomes more and more flattened. This effect is known as the "Hartmann effect". The thin layer near the wall where the flow velocity changes from zero to U_m is called the "Hartmann layer". The Hartmann effect is caused by the lorentz force, which accelerates the fluid in the Hartmann layers and slows it down in the bulk.

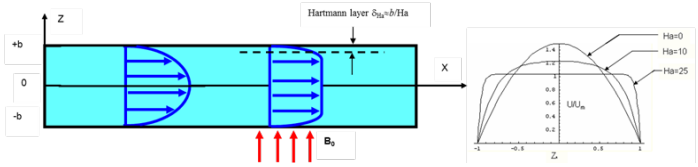

Figure 5 Hartmann solutions.

Hartmann solution is

$$\frac{U}{U_m} = \frac{\mathrm{Ha}}{\mathrm{Ha} - \tanh \mathrm{Ha}}\left[1 - \frac{\cosh(\mathrm{Ha}\times z_*)}{\cosh \mathrm{Ha}}\right] \qquad (24)$$

Hunt[13] and Hunt et al.[14] reported on MHD flows in rectangular ducts. A rectangular duct study was done in Fluent a commercial code as shown in Figure 6.

Here, 2a = 424 mm in toroidal direction, 2b = 50 mm in radial direction and L = 1455 mm in poloidal direction of the fusion reactor.[15,16] The following are assumed: Alumina coating used for perfect insulation with conductivity of the order of 10^{-8} 1/Ω-m, there is no electromagnetic coupling between adjacent flow channels of Pb-Li, the flow is fully developed flow inside the channels due to the length of the channels, due to high Interaction parameter, turbulence is suppressed by MHD phenomena and that there are no cracks are present in the alumina coating or alumina is capable of self-healing. The mesh work of the simulation model is shown in Figure 7.

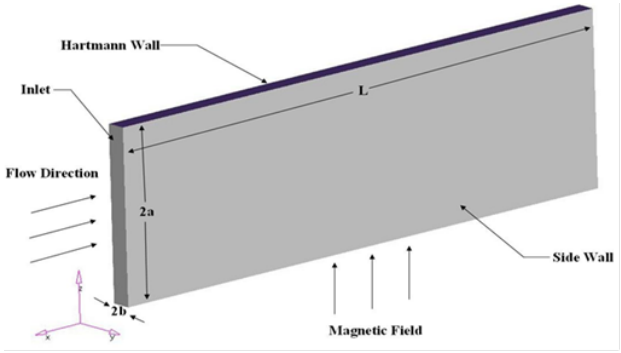

Figure 6 Computer simulation model for Pb-Li flow study in tritium breeding module.

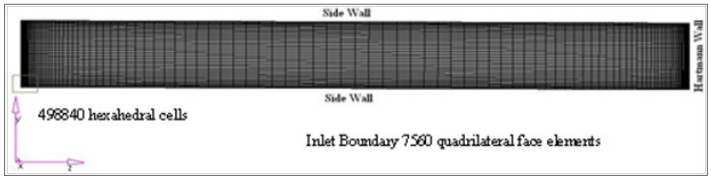

Figure 7 Mesh work of the simulation model.

Fine mesh near the Hartmann walls is used, Ha for the present case used is 20000, i.e.,

$$\delta_H = \mathrm{Ha}^{-1} = \frac{1}{20000} = 0.00005 \text{ m} \qquad (25)$$

So four cells were maintained below the distance of 0.00005m from the Hartmann walls. Thickness of side wall boundary layer

$$\delta_S = \mathrm{Ha}^{-1/2} = \frac{1}{20000^{1/2}} = 0.007 \text{ m} \qquad (26)$$

Mesh near the Hartmann wall on inlet is shown in Figure 8. Table 1 gives the material properties used in the simulation.

Table 1 Material properties

	Lead-lithium	Alumina	FMS
Density (kg/m³)	8430	3890	7871
Electrical Conductivity (1/Ω-m)	750000	-	1385041
Dynamic Viscosity (kg/m-s)	0.0016	-	-
Thermal Conductivity (W/m-K)	14.8	35	33
Specific Heat (J/kg-K)	188.088	880	570

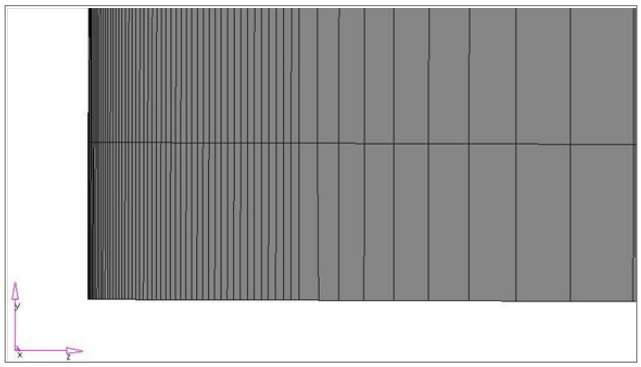

Figure 8 Mesh near the Hartmann wall on inlet.

Total pressure loss (Figure 9) from friction and magnetic effects together is 95.157 + 15.12 = 110.277 Pa and agrees well with the analysis of Hunt.[12,13]

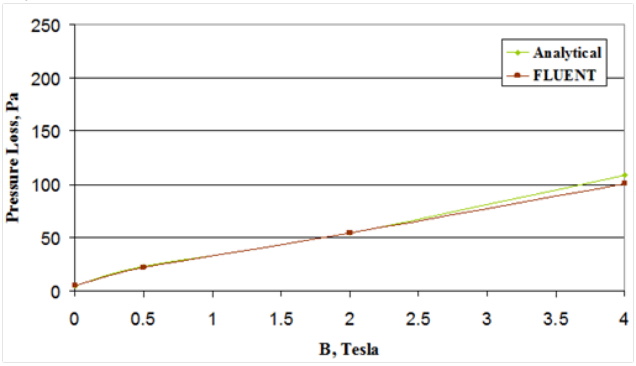

Figure 9 Comparison of results - pressure loss.

In the presence of magnetic field U_x reaches U_m in a very short distance of the order of 10^{-5} m, whereas in the absence of magnetic field the peak is reached around the middle as shown in Figures 5 and Figure 10. This makes the meshing of MHD flows dense near the Hartmann walls.

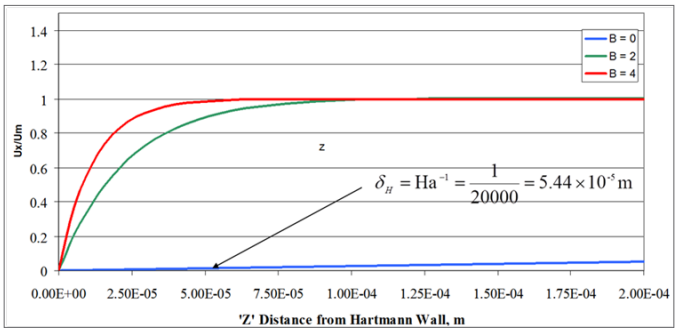

Figure 10 Comparison of Results - U_x/U_m near Hartmann wall in z direction.

Finally we show the results obtained for Hartmann layer thickness for two different values of B = 2 and 4 in Figure 11.

Heat transfer coefficients are given in Table 2 in radial and toroidal directions and overall values.

Table 2 Heat transfer coefficients in three directions

	HTC radial	HTC toroidal	HTC overall
B = 0 (Laminar)	357.12	1118.04	1037.77
B = 0 (K-e)	918.73	2431.82	2272.21
B = 2 (Laminar)	2205.47	1195.47	1248.25
B = 4 (Laminar)	2180.58	547.68	694.52

As Hartmann number increases, the overall heat transfer coefficient decreases due to suppression of turbulent pulsation. This results in reduction of transport of thermal properties. As convective heat transfer is due to transport of thermal properties, the value of heat transfer coefficient will also be less at high Hartmann numbers. The heat transfer coefficient value on the Hartmann wall increases, because the velocity gradients near the Hartmann wall increases which promote turbulent mixing.

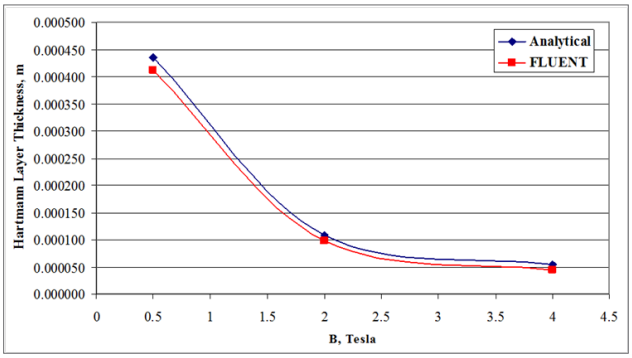

Figure 11 Comparison of results - hartmann layer thickness.

Governing equations for aero-acoustics in flow

The linearized wave equation that governs wave propagation of small amplitude waves in a stationary ideal fluid is given by

$$\nabla^2 p - \frac{1}{c^2}\frac{\partial^2 p}{\partial t^2} = 0 \tag{27}$$

where c is speed of wave propagation and in atmospheric air at 0°C given by

$$c = \sqrt{\frac{\gamma p_0}{\rho_0}} = \sqrt{\frac{1.4\times10^5}{1.2}} = 331.6 \text{ m/s} \tag{28}$$

The non-homogenous wave equation containing a source term q is

$$\frac{\partial^2 p}{\partial t^2} - c^2\nabla^2 p = q \tag{29}$$

Often we will consider situations where the source q is concentrated in a limited region of space embedded in a stagnant uniform fluid. Let us choose the fluctuating part ρ as acoustic variable, and then we can write the wave equation (27) as

$$\frac{\partial^2 \rho'}{\partial t^2} - c^2\nabla^2 \rho' = 0 \tag{27a}$$

The nonhomogeneous form of continuity equation (1) is

$$\frac{\partial \rho}{\partial t} + div(\rho\,\mathbf{U}) = m \tag{1a}$$

where the source m consists of mass of density ρ_m of volume fraction $\beta = \beta(\mathbf{x}, t)$ injected at a rate

$$m = \frac{\partial}{\partial t}(\beta\rho_m) \tag{3a}$$

The source region is where $\beta \neq 0$ in equation (1a).

Since the injected mass displaces the original mass ρ_f by the same (but negative) amount of volume, the total fluid density is

$$\rho = \beta\rho_m + (1-\beta)\rho_f \tag{30}$$

where the injected matter does not mix with the original fluid. Substitute the above in (3) and eliminate $\beta\rho_m$

$$\frac{\partial}{\partial t}\rho_f + \nabla\cdot(\rho\mathbf{V}) = \frac{\partial}{\partial t}(\beta\rho_f) \tag{31}$$

Using a linearized form of the equation of momentum conservation $\frac{\partial}{\partial t}(\rho\mathbf{V}) + \nabla p' = f$, the above equation (31) can be rearranged as

$$\frac{\partial^2}{\partial t^2}\rho_f - \nabla^2 p' = \frac{\partial^2}{\partial t^2}(\beta\rho_f) - \nabla\cdot f \tag{31a}$$

If we assume, for simplicity, that $p' = c_0^2 \rho_f'$ everywhere, where ρ_f' is the fluctuating part of ρ_f which corresponds to the sound field outside the source region, then

$$\frac{1}{c_0^2}\frac{\partial^2}{\partial t^2}p' - \nabla^2 p' = \frac{\partial^2}{\partial t^2}\left(\beta\rho_f\right) - \nabla \cdot f \tag{31b}$$

Comparing with (29) we find the source term is $c_0^2\left[\frac{\partial^2}{\partial t^2}\left(\beta\rho_f\right) - \nabla \cdot f\right]$ which shows that mass injection is a source of sound, primarily because of the displacement of a volume fraction β of the original fluid ρ_f

Lighthill[8] introduced the notion of "analogy" of representing a complex fluid mechanical process that acts as an acoustic source by an acoustically equivalent source term. The notion of "analogy" refers here to the idea of representing a complex fluid mechanical process that acts as an acoustic source by an acoustically equivalent source term. While Lighthill's equation is formally exact (i.e. derived without approximation from the navier-stokes equations), it is only useful when we consider the case of a limited source region embedded in a uniform stagnant fluid. At least we assume that the listener which detects the acoustic field at a point x at time *t* is surrounded by a uniform stagnant fluid characterized by a speed of sound c_0. Hence the acoustic field at the listener should accurately be described by the wave equation (27a). The key idea of the so-called "aero-acoustic analogy" of Lighthill is to derive from the exact equations of motion a non-homogeneous wave equation with the propagation part as given by (27a). Hence the uniform stagnant fluid with sound speed c_0, density ρ_0 and pressure p_0 at the listener's location is assumed to extend into the entire space, and any departure from the "ideal" acoustic behavior predicted by (27a) is equivalent to a source of sound for the observer. By taking the time derivative of the mass conservation law (1a) and eliminating $\partial m/\partial t$

$$\frac{\partial^2}{\partial t \partial x_i}\left(\rho u_i\right) = \frac{\partial m}{\partial t} - \frac{\partial^2 \rho}{\partial t^2} = -\frac{\partial^2 \rho_f}{\partial t^2} + \frac{\partial^2 \beta\rho_f}{\partial t^2} \tag{32}$$

By taking the divergence of the momentum conservation law (1a) and substituting in above

$$\frac{\partial^2 \rho_f}{\partial t^2} = \frac{\partial^2}{\partial x_i \partial x_j}\left(P_{ij} + \rho u_i u_j\right) + \frac{\partial^2 \beta\rho_f}{\partial t^2} - \frac{\partial f_i}{\partial x_i} \tag{33}$$

Here velocity and pressure are decomposed $\mathsf{v} = \mathsf{V} + \mathsf{v}'$ and $p = P + p'$. Because $\rho_f = \rho_0 + \rho'$ where only ρ' varies in time we can construct a wave equation for ρ' by subtracting from both sides of (33) a term $c_0^2 \frac{\partial^2 \rho'}{\partial x_i^2}$ where in order to be meaningful c_0 is not the local speed of sound but that at the listener's location. Lighthill's equation is

$$\frac{\partial^2 \rho'}{\partial t^2} - c_0^2 \frac{\partial^2 \rho'}{\partial x_i^2} = \frac{\partial^2 T_{ij}}{\partial x_i \partial x_j} + \frac{\partial^2 \beta\rho_f}{\partial t^2} - \frac{\partial f_i}{\partial x_i} \tag{34}$$

where Lighthill's stress tensor T_{ij} is defined by

$$\begin{aligned} T_{ij} &= \left(P_{ij} + \rho u_i u_j\right) - \left(c_0^2 \rho' + p_0\right)\delta_{ij} \\ &= \rho u_i u_j - \tau_{ij} + \left(p' - c_0^2 \rho'\right)\delta_{ij} \end{aligned} \tag{35}$$

In equation (35) above $P_{ij} = p\delta_{ij} - \tau_{ij}$ is used and we distinguish three basic aero-acoustic processes which result in sources of sound:

Non-linear convective forces described by the Reynolds stress tensor, $\rho u_i u_j$

Viscous forces τ_{ij}

Deviation from a uniform sound velocity c_0 or the deviation from an isentropic behavior $\left(p' - c_0^2 \rho'\right)$.

It can be shown that the effect of a rigid body can be incorporated in the aero-acoustical analogy of Lighthill as additional source and force terms Q_m and $\boldsymbol{F}$. This approach has been generalized, see Ffowcs Williams et al.[9] who derived a very general formulation valid for any moving body, enclosed by a surface S*(t)*. Although originally meant to include the effect of moving closed surfaces into Lighthill's theory for aerodynamic sound, it is now a widely used starting point for theories of noise generation by moving bodies like propellers, even when turbulence noise is of little or no importance. Ffowcs Williams and Hawking's equation is

$$\frac{\partial^2 \rho'}{\partial t^2} - c_0^2 \frac{\partial^2 \rho'}{\partial x_i^2} = \frac{\partial^2 T_{ij}}{\partial x_i \partial x_j} - \frac{\partial}{\partial x_i}\left[(p'\delta_{ij})\frac{\partial f}{\partial x_j}\delta(f)\right] + \frac{\partial}{\partial t}\left[\rho_0 u_i \frac{\partial f}{\partial x_i}\delta(f)\right] \tag{36}$$

The definition of surface *f=0 i*s given in Figure 12.

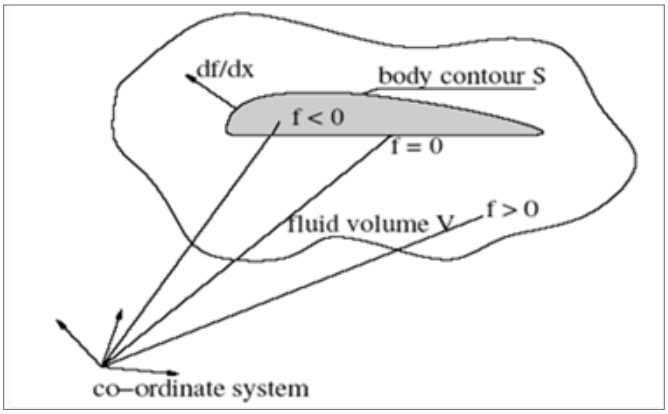

Figure 12 Definition of surface f = 0.

In equation (36) the right hand side terms in order are

1. T_{ij} ~ Lighthill's stress tensor which contains velocity variations related acoustic source terms (Quadrupole) and entropy acoustic source terms
2. Dipole sources are due to pressure variations at physical solid surface
3. Monopole sources are due to displacements of fluid by accelerating/decelerating surfaces.

The solution of wave equation can be easily obtained. A monopole represents volume velocity or volume displacement sources. Instantaneous pressure field in an ideal spherical wave from a monopole is illustrated in Figure 13, where the fluid is air (*c*=344 m/s) and the frequency is 1000 Hz. Source is 10 cm dia. Maximum positive pressure is blue, and minimum (negative) pressure is red zero pressure is blue/green.

Dipole is a pair of closely spaced Monopoles; a point force is directed along the Dipole axis. While a Monopole can be considered as a Mass source, a Dipole is a force source. Fluid-solid interaction

and boundary layer turbulence are typically dipole like. The radiated pressure from an ideal dipole is given in Figure 14. The frequency here is 500 Hz and the source dia is 8 cm; one source is at $(x,y)=(0,0)$ and the other at $(x,y)=(0.1,0)$, dipole moment $k_d=0.91$.

A point quadrupole is an array of two dipoles, there is no net force and it exerts an oscillating moment as in oscillatory rotation in turbulent flows. The radiated pressure from an ideal Quadrupole is shown in Figure 15. The frequency is 500 Hz, source diameter is 8 cm; sources at $(x,y)=(0,0)$, $(0.1,0)$, $(0,0.1)$, and $(0.1,0.1)$ and Quadrupole moment $(k_d)^2=0.81$.

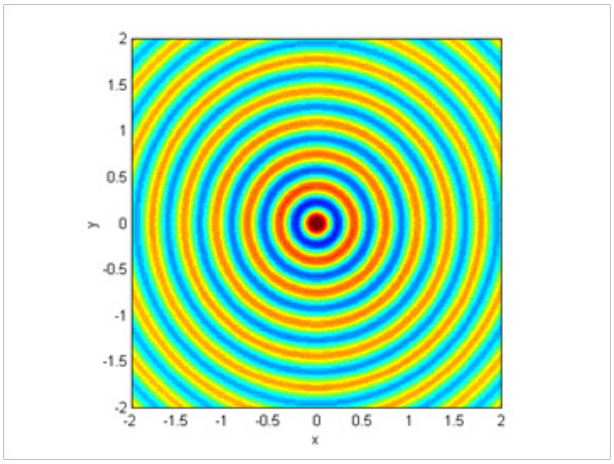

Figure 13 Monopole.

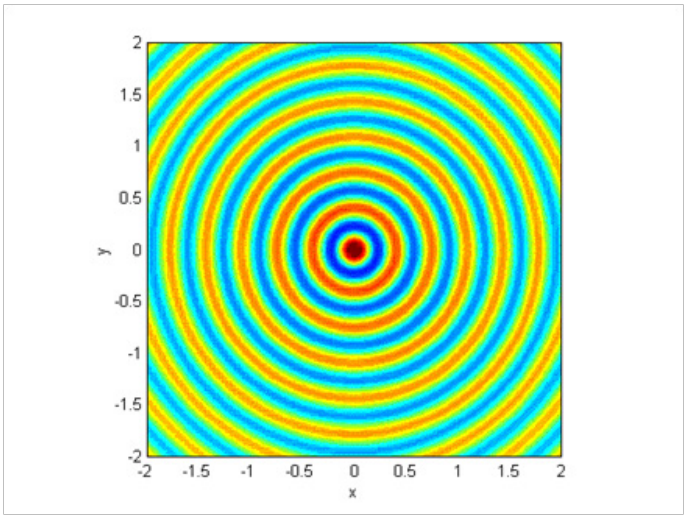

Figure 15 Quadrupole.

Flow over a cylinder

As a simple example, we consider 2D flow over a 0.19m dia cylinder in Figure 17. The inlet velocity is 69.2m/s. Strouhal number $S_t = f_s D/U$ is 0.22 and frequency of shedding f_s = 821Hz.[17] The meshwork is shown in Figure 18. For simplicity 120,000 grids are adopted. As discussed in previous sections, LES turbulence model is used for turbulence modeling.

Fluent is used to solve the pressure distribution and the sound levels at the listener's location shown. The velocity magnitude contours, which show the eddies shed in the downstream flow, are given in Figure 19.

The fluid flow problem represented by RANS equations and appropriate turbulence models is first solved by finite volume method to capture the flow phenomenon giving rise to the noise. The Ffowcs-Hawking equations are then solved by capturing the sources from the flow to obtain the noise signature. Because of the complexity of the real life problems it is not possible to attempt solutions in conventional manner; instead well-established codes can be practiced. The flow field solution can be captured first in a numerical solver and the pressure fronts can be transferred to noise solver. The overall approach can be summarized as given in Figure 16.

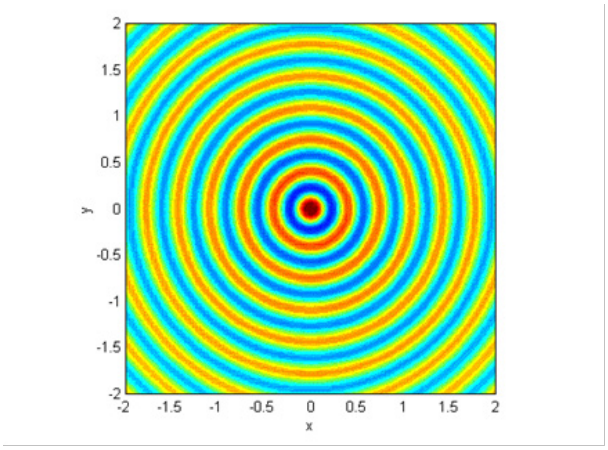

Figure 14 Dipole.

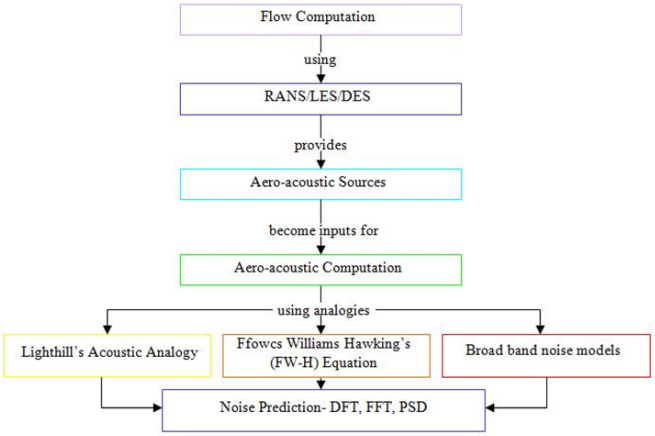

Figure 16 Solution approach for aero-acoustics.

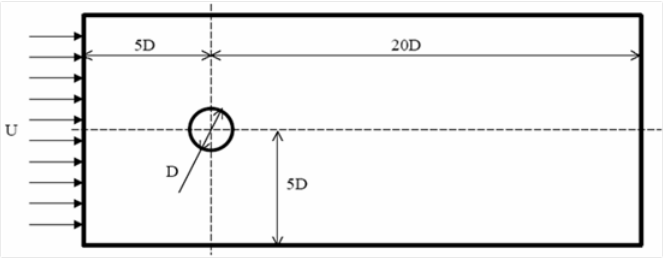

Figure 17 Computational domain of flow over a cylinder.

The result obtained for Sound Pressure Level as a function of Strouhal number is given in Figure 20. The strouhal number obtained from Fluent agrees well with calculation. Figure 21 shows the power spectral density and the peak obtained is at 821 Hz which is in good agreement with exact value.

Noise in two phase flow under rocket lift-off conditions

The domain description is given in Figure 22. The mesh work (2D) is shown in Figure 23. This meshwork should be sufficiently fine to capture two phase flow with nitrogen and air. The grid in the present case is 150,000 cells only. The velocity magnitude contours showing the vortices is illustrated in Figure 24. The sound pressure level is given in Figure 25 and the acoustic pressure in time domain is shown in Figure 26.

Cavity acoustics

In the previous examples pressure surfaces were picked up as sources to determine the flow noise. Here noise in enclosures is illustrated. Typically an enclosure acts as a resonator. When the acoustic modes coincide with a given frequency in the spectrum we get amplified noise. A door gap cavity is shown in Figure 27.

A CFD analysis with LES turbulence model is performed to determine the vorticity contours as shown in Figure 28. As the airflow hits the cavity its boundary layer is broken and eddies are shed in the downstream. These eddies interact with the flow in the cavity and produce resonance at some frequencies. The acoustic pressure sources are captured as illustrated in Figure 29. Figure 30 shows the sound pressure level in the cavity. Figure 31 shows the power spectral density that peaks at a frequency close to 2500 Hz corresponding to the frequency in Figure 30.

Practical applications of such cavities are sun roof in an automobile, Here Ahmed's body, a standard bench mark, is shown in Figure 32. Figure 33 shows the velocity contours following the procedure outlined in Figure 19. One can optimize the cavity location and shape to reduce the noise inside the vehicle.

Another application is shown in an aircraft cockpit shown in Figure 34 with the flow path obtained from Fluent. Figure 35 shows the acoustic pressure in time domain in the cockpit and sound pressure level components in dB at the pilot's ear location in the cockpit are shown in Figure 36. Here again one can optimize the cock pit shape to reduce the sound pressure level at the pilot's here to enable him comfortably bear the high noise levels to be within acceptable standards.

The optimization process is not dealt here and should follow the noise studies and make the sound pressure level at the receiver location as an objective function along with the constraints.

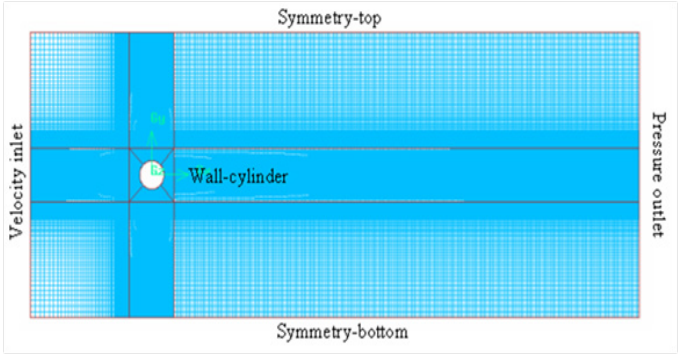

Figure 18 Mesh work in the flow domain.

Figure 19 Velocity contour paths showing the shed eddies.

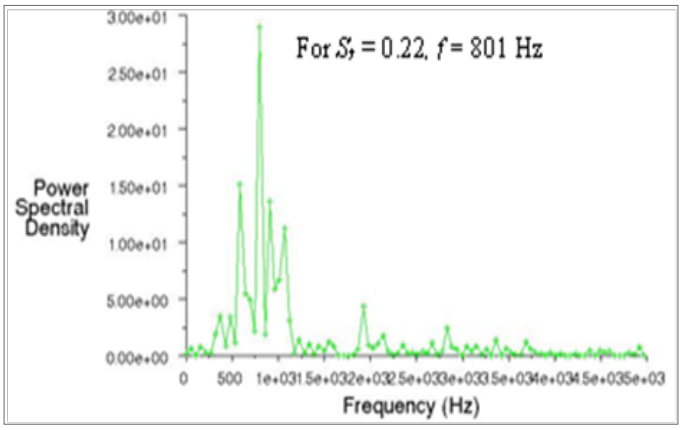

Figure 20 Sound pressure level.

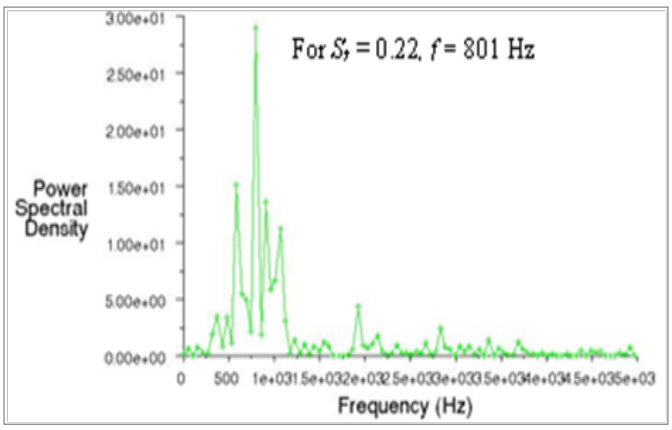

Figure 21 Power Spectral Density peaks at 801 Hz.

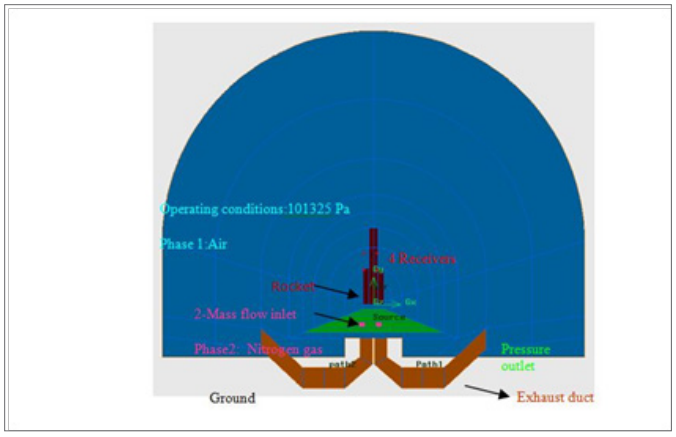

Figure 22 Two Phase Flow under Rocket Lift Off Conditions.

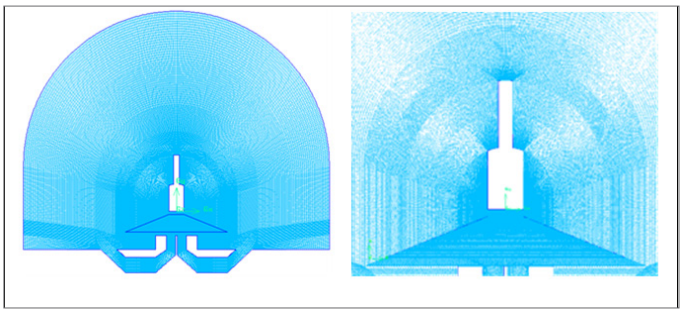

Figure 23 Mesh work.

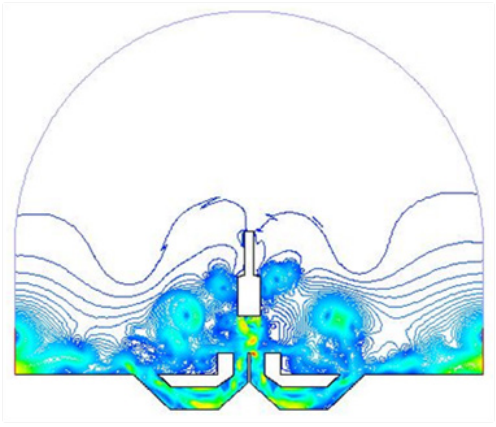

Figure 24 Velocity magnitude contours.

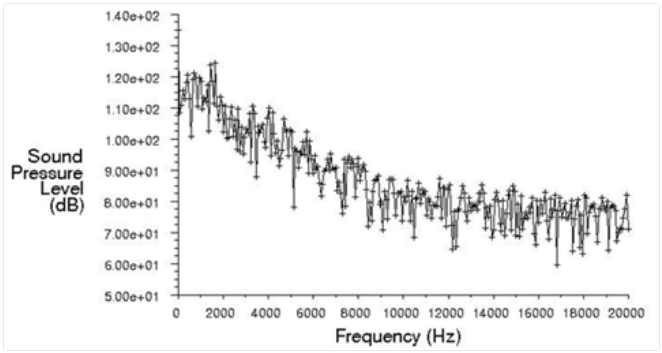

Figure 25 Sound pressure level.

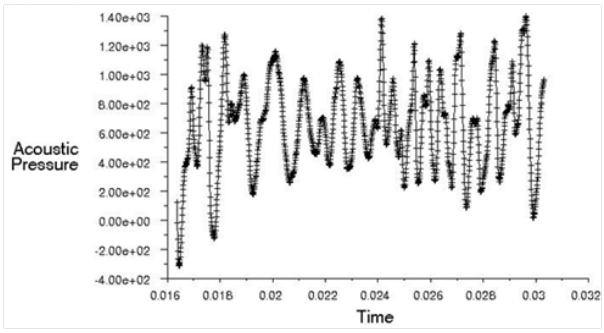

Figure 26 Acoustic pressure in time domain.

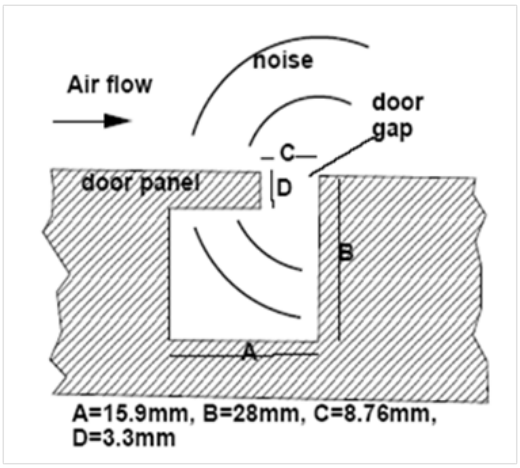

Figure 27 A door panel with cavity.

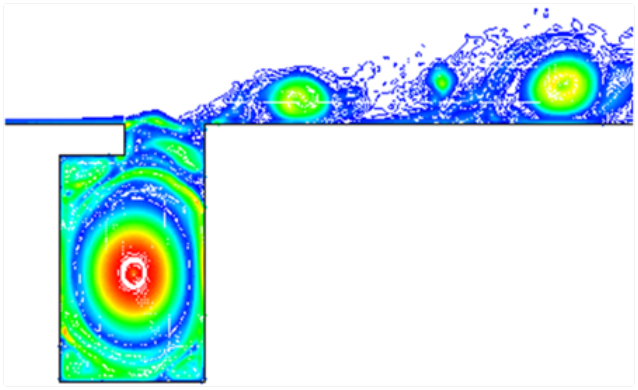

Figure 28 Vorticity contours.

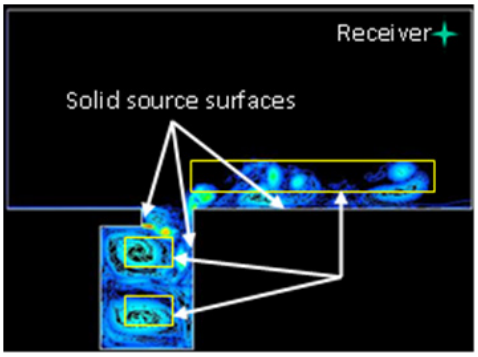

Figure 29 Capturing of acoustic source surfaces.

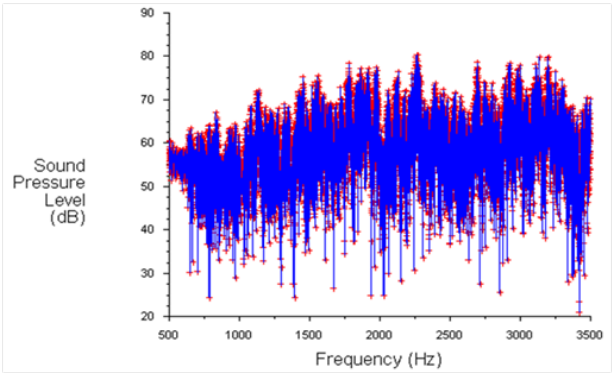

Figure 30 Sound pressure level in the cavity.

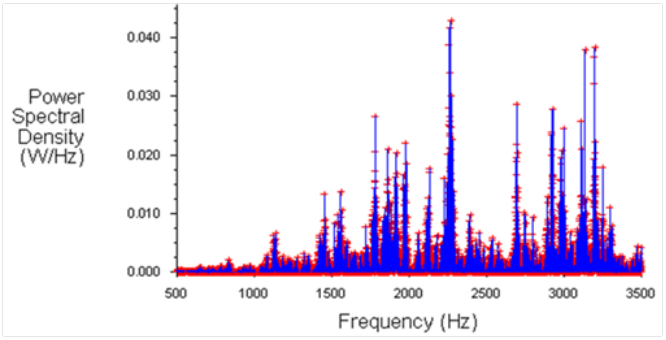

Figure 31 Power spectral density in the cavity.

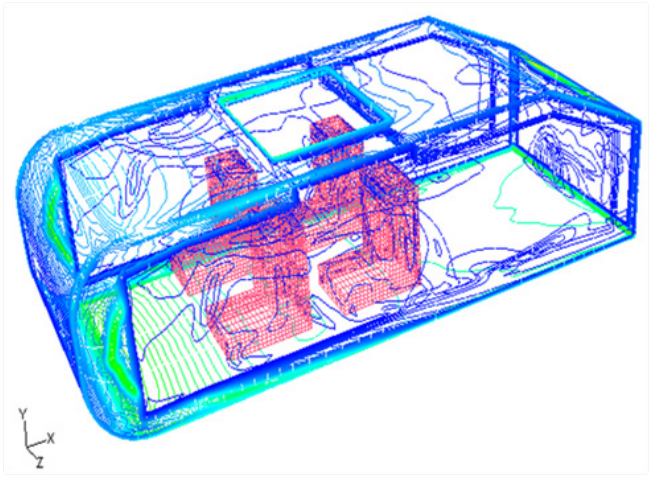

Figure 32 Velocity contours in ahmed body cavity.[18]

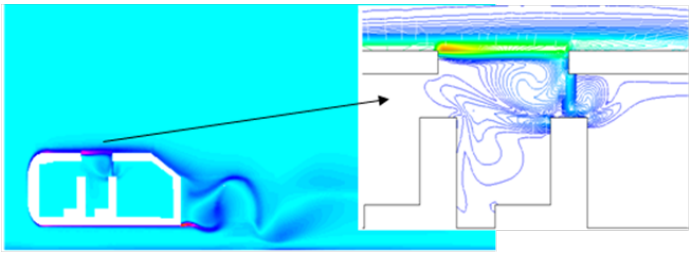

Figure 33 Vorticity contours.

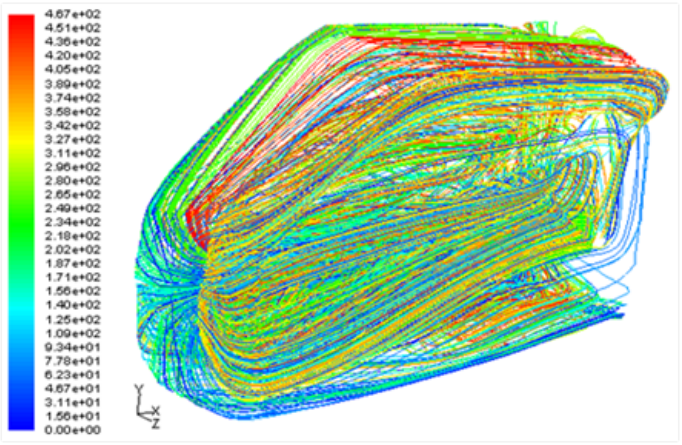

Figure 34 Cock pit flow path.

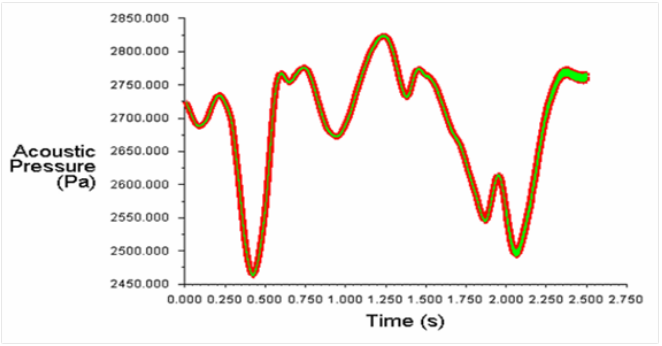

Figure 35 Acoustic pressure in time domain in the cockpit.

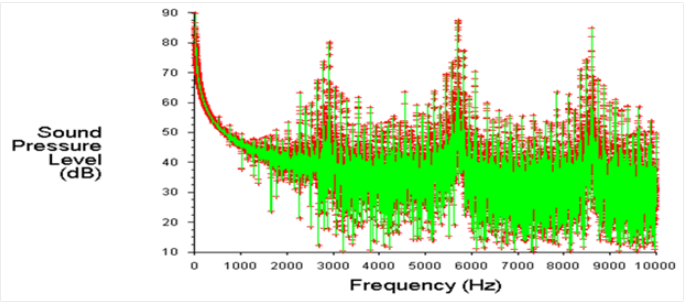

Figure 36 Sound pressure level components in the cockpit.

Conclusion

In this paper complex fluid flow problems were considered by Simulation Based Engineering approach using modern commercial CFD codes with multi-physics capability.

The governing equations for MHD flows are given with applications to fusion reactor liquid lithium flow problems are considered. The Hartmann layer prediction with dense mesh is shown to predict theoretical values of simple geometry.

Wave propagation and noise prediction from the flow is also illustrated in the paper. Lighthill's analogy and Ffowcs Williams-Hawking's approach for sound generated by turbulence and surfaces in arbitrary motion is also illustrated together with practical examples

of Blevins flow over circular body and launch vehicle external flows. Internal flow of cavities, aircraft cockpits, is also given as obtained from today's Science to Engineering approach.

With the current capabilities any complex flow problem can be attempted with SBES and high performance computing.

Acknowledgements

So many students, colleagues in different countries have helped me during nearly six decades in achieving success of considerable works and projects. I am highly indebted to them.

Ever since we were married in 1962, my wife stood by my side is supporting my work. I am indebted to her devotion to family and help. We have a great grandson and looking forward to second great grandchild to bring joy into our lives.

Conflict of interest

Authors declare there is no conflict of interest in publishing the article.

References

1. Euler L. Principes généraux du mouvement des fluids. Mémoires de l'académie des sciences de berlin. Berlin: Germany; 1757. P. 274–315.
2. Navier L, de l'équilibre et du mouvement des corps solides élastiques, Paper read to the Académie des Sciences. 1821.
3. Stokes GG. On the theories of the internal friction of fluids in motion, and of the equilibrium and motion of elastic solids. *Cambridge philosophical society transactions*. 1849;8:287.
4. Faraday Michael. Experimental Researches in Electricity. vols I & II. Richard and John Edward Taylor vol III. Richard Taylor and William Francis. 1855.
5. Reynolds O. On the dynamical theory of incompressible viscous fluids and the determination of the criterion. *Proceedings of the royal society*. 1894;56:336.
6. Alfven H. Existence of electromagnetic-hydrodynamic waves. *Nature.* 1942;150:405−6.
7. Rao JS, Sankar H. Magneto Hydro-Dynamics and Heat Transfer in Liquid Metal Flows. *Developments in heat transfer*. 2011;4:55−80.
8. Lighthill MJ. On sound generated aerodynamically II. Turbulence as a source of sound. *Proceedings of the royal society*. 1954;(1148):1–32.
9. Ffowcs Williams JE, Hawkings DL. Sound generated by turbulence and surfaces in arbitrary motion. *Philosophical transactions of the royal society of london*. 1969;264(1151):321–42.
10. Rao JS. Creativity in design - science to Engineering Model, MAMT3006. *Mechanism and Machine Theory*. 2018;125:52–79
11. Hartmann J. Theory of the laminar flow of electrically conductive liquid in a homogeneous magnetic field. *Hg-Dynamics 1*. 1937;15(6):1–28.
12. Hartmann J, Lazarus P. Experimental investigation of flow of Mercury in a homogeneous magnetic field. *Hg-Dynamics II*. 1937;15(7):1–46.
13. Hunt JCR. Magneto hydrodynamic flow in rectangular ducts. *Journal of fluid mechanics*. 1965;21(4):577–590.
14. Hunt JCR, Stewartson K. Magneto hydrodynamic flow in rectangular ducts. II. *Journal of fluid mechanics*.1965;23(3):563–581.
15. Rao JS, CPC wong, M abdou, et al. Design description document for the dual coolant Pb 17Li (DCLL) test blanket module, Report to the ITER test blanket working group (TBWG). Institute of Plasma Research, India. 2005. p. 1–206.
16. Rao JS, Sankar H. Numerical simulation of MHD effects on convective heat transfer characteristics of flow of liquid metal in annular tube. *Journal of fusion engineering and design*. 2011;86(2-3):183–191.
17. Blevins RD. Flow-induced vibration. 2nd edition. New York: Van Nostrand Reinhold;1990. p. 451.
18. Ahmed SR, Ramm G, Faltin G. Some salient features of the time-averaged ground vehicle wake. SAE International congress and exposition. 1984. p. 34.